Structure of a Quinobenzoxazine−G-Quadruplex Complex by REDOR NMR

Anil K. Mehta,[‡] Yuda Shayo,[§] Hariprasad Vankayalapati,[§] Laurence H. Hurley,[§] and Jacob Schaefer*[,‡]

Department of Chemistry, Washington University, St. Louis, Missouri 63130, and College of Pharmacy, University of Arizona, Tucson, Arizona 85721

Received February 10, 2004; Revised Manuscript Received July 12, 2004

ABSTRACT: Rotational-echo double resonance solid-state $^{31}P\{^{19}F\}$ and $^{13}C\{^{19}F\}$ NMR spectra have been used to locate the binding of a fluoroquinobenzoxazine to a DNA G-quadruplex labeled by phosphorothioation and [methyl-^{13}C]thymidine.

G-quadruplexes are conformations of guanine-rich DNA resulting from the association of sets of four guanine residues into planar arrays (*1*). G-quadruplexes were first suggested as potential targets for drug design 15 years ago (*2*). Recently, G-quadruplex-interactive compounds have been shown to inhibit telomerase in both cell-free and in vitro systems (*3*−*5*), cause telomere shortening and cell crisis in cancer cells (*6*) and lower c-*MYC* gene expression by targeting transcriptional control (*7*).

G-quadruplexes can be modeled in vitro by aggregation of four parallel 5′−3′ single strands of DNA (*8*), each with the sequence TAG_3T_2A (similar to the human telomeric repeat T_2AG_3). This system forms G-tetrad planes and binds drugs that are known to inhibit telomerase (*9*). Solution-state ^{1}H NMR detection of G-base chemical shifts indicated quadruplex formation and binding of a fluorine-substituted quinobenzoxazine (QQ58,[1] bottom of Figure 1). The more pronounced upfield shift of the G5 imino proton relative to those of G4 and G3 suggested that the site of QQ58 binding (*9*, *10*) is between G5 and T6 (top of Figure 1). However, the absence of any NOE contacts to the drug (presumably the result of unfortuitous dynamics) precluded a structural determination. Diffraction-quality crystals of the complex are not available.

In this paper, we report the use of 202-MHz $^{31}P\{^{19}F\}$ and 125-MHz $^{13}C\{^{19}F\}$ rotational-echo double resonance (REDOR) NMR (*11*) to help establish the mechanism of binding of the fluoroquinobenzoxazine. Solution-state dynamics are suppressed in the solid state, and this allows the direct measurement of dipolar couplings (and hence distances) between the fluorine of QQ58 and nearby ^{13}C and ^{31}P labels (the latter generated by phosphorothioation). The ultimate goal of this paper is to provide sufficient molecular detail of the mode of binding of QQ58 to allow the design of analogues that differentiate between duplex and G-quadruplex DNA-binding sites.

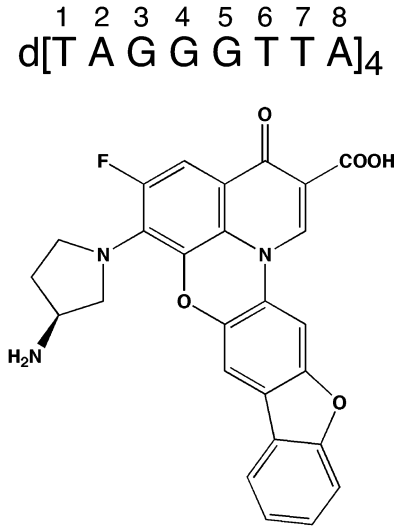

FIGURE 1: (Top) Sequence and numbering of the oligomer used in this study. (Bottom) Structure of QQ58.

MATERIALS AND METHODS

Synthesis of Fluoroquinolone (QQ58) and Quadruplex DNA. The fluoroquinolone was synthesized as described in Duan et al. (*10*). Oligonucleotides were synthesized on a PerSeptive Biosystems Expedite 8909 automatic DNA synthesizer. Phosphorothioate linkages were introduced at two sites, between G4 and G5 (TAGGsGTTA) and between G5 and T6 (TAGGGsTTA). The latter also contained [methyl-^{13}C]thymidine at T6. The oligonucleotide numbering scheme (top of Figure 1) is that of Duan et al. (*10*). Samples were purified by reverse-phase liquid chromatography on a C18 column (Dynamax-300A) and dialyzed extensively against 10 mM KCl followed by deionized water.

REDOR. REDOR was used to restore the dipolar couplings between heteronuclear pairs of spins that are removed by magic-angle spinning (*11*). REDOR experiments are always done in two parts, once with rotor-synchronized dephasing pulses (S) and once without (S_0). The dephasing pulses change the sign of the heteronuclear dipolar coupling, and this interferes with the spatial averaging resulting from the

* To whom correspondence should be addressed: Department of Chemistry, Washington University, One Brookings Drive, St. Louis, MO 63130. Telephone: 314-935-6844. Fax: 314-935-4481. E-mail: schaefer@wuchem.wustl.edu.

‡ Washington University.

§ University of Arizona.

[1] Abbreviations: MCT model, a computer model of a quadruplex complex that appeared in *Mol. Cancer Ther.*; NMR model, the REDOR-refined MCT model; QQ58, a fluoine-substituted quinobenzoxazine; REDOR, rotational-echo double resonance.

10.1021/bi049697h CCC: $27.50
Published on Web 08/28/2004

motion of the rotor. The difference in signal intensity ($\Delta S = S_0 - S$) for the observed spin in the two parts of the REDOR experiment is directly related to the corresponding distance to the dephasing spin. REDOR has found an application in the characterization of binding sites of proteins (*12*−*14*) and in the analysis of heterogeneous biological materials such as amyloid plaques (*15*), membrane protein helical bundles (*16*), and bacterial cell walls (*17*).

Spectrometer. REDOR NMR was performed using a 6-frequency transmission-line probe (*18*) having a 12-mm long, 6-mm inside-diameter analytical coil and a Chemagnetics/Varian ceramic stator. Lyophilized samples were contained in thin-wall Chemagnetics/Varian 5-mm outside-diameter zirconia rotors. The rotors were spun at either 7143 or 7463 Hz with the speed under active control to within ±2 Hz. A stack-mounted air chiller cooled the rotor to an exit-gas temperature of −10 °C. The spectrometer was controlled by a Tecmag pulse programmer. Radio frequency pulses for ^{31}P (202 MHz) and ^{13}C (125 MHz) were produced by 1-kW American Microwave Technology power amplifiers. Proton (500 MHz) and ^{19}F (470 MHz) radio frequency pulses were generated by 1-kW Amplifier Systems tube amplifiers driven by 50-W American Microwave Technology power amplifiers. The π-pulse lengths were 10 μs for ^{31}P, 8 μs for ^{13}C, and 5.0 μs for ^{19}F. The ^{31}P spectra were acquired with a sweep width of 20 times the spinning frequency.

^{31}P{^{19}F} REDOR spectra were collected with a single ^{31}P refocusing pulse (to avoid phase distortions resulting from ^{31}P−^{31}P coupling) and standard xy-8 phase cycling (*19*) for all dephasing ^{19}F pulses; ^{13}C{^{19}F} spectra were collected with xy-8 phase-cycled π pulses on both the ^{13}C and ^{19}F channels (*20*). A 12-T static magnetic field was provided by an 89-mm bore Magnex superconducting solenoid. Proton-phosphorus cross-polarization transfers were made in 1 ms for TAGGGsTTA and 5 ms for TAGGsGTTA with radio frequency fields of 50 kHz. Proton-carbon cross-polarization transfers were made in 2 ms with radio frequency fields of 62.5 kHz. Proton dipolar decoupling was 100 kHz during data acquisition; TPPM of the ^{1}H radio frequency (*21*) was used throughout both dipolar evolution and decoupling periods.

REDOR Sample. Formation of a quadruplex−drug complex was confirmed by solution-state ^{1}H NMR. The solutions were then frozen and lyophilized in the presence of 1 mM poly(etheylene glycol) as a cryoprotectant. About 10 mg of the dry complex was mixed with 100 mg of sulfur and pressed into a single pellet whose diameter matched that of the inside diameter of the rotor. The pellet was held under vacuum for a week and then inserted into the rotor in a glovebox under a nitrogen atmosphere. The rotor was sealed on both ends with pressed molecular-sieve disks (15 mg each) and veined Kel-F end caps to avoid the uptake of water.

Model Building and Molecular Dynamics Simulations. The initial coordinates used in the model-building process were those published for the solution-state NMR-based model of the 1:1 PIPER:5′-d[TAG$_3$T$_2$A]$_4$-3′ complex (*9*) and the antiparallel human telomeric sequence d[AG$_3$(T$_2$AG$_3$)$_3$] (*22*). The necessary replacements and the addition of hydrogens were carried out using INSIGHT II (Insight II; Molecular Simulations Inc., San Diego, CA). Positions were refined by energy minimization (1000 cycles of steepest descent and 2 × 1000 cycles of conjugate-gradient minimization) while

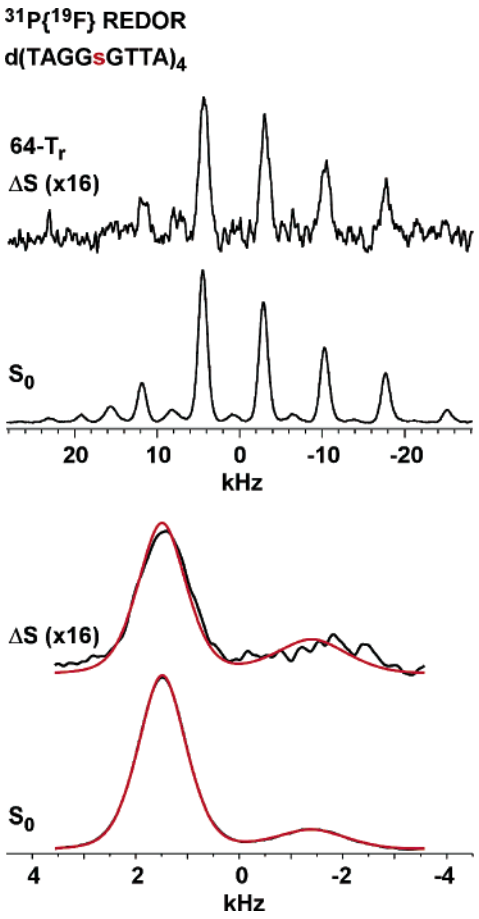

FIGURE 2: ^{31}P{^{19}F} REDOR NMR spectra (202 MHz) of the complex of QQ58 with a sulfur-tagged quadruplex. The top two spectra show sidebands resulting from magic-angle spinning at 7463 Hz after 64 rotor cycles of dipolar evolution. The full-echo spectrum (no dephasing) is labeled S_0 and the REDOR difference spectrum (the difference between echo spectra with and without dephasing), ΔS. The major set of peaks in each spectrum is due to PO_4 and the minor set, to PO_3S. Digitizing of the NMR signal was done at 20 times 7463 Hz so that the Fourier transform of every 20th time-domain data point resulted in the bottom two spectra. These spectra have center- and sidebands folded together in a window whose width is the spinning frequency. The major peak on the left is due to $^{31}PO_4$, and the minor peak on the right is due to $^{31}PO_3S$. The relative positions of the two peaks were determined by the choice of the radio frequency carrier offset. The true centerband frequency of the $^{31}PO_3S$ is greater (to the left in the top two spectra) than that of the $^{31}PO_4$ peak by 56 ppm (11.3 kHz). Integrated intensities were measured from the Lorentzian line fits shown in red. The G-quadruplex−drug complex weighed about 8 mg and represented about 0.8 μmol of binding sites. Data acquisition required 5 days of spectral accumulation.

constraining the positions of heavy atoms. Finally, the entire structure was subjected to conjugate-gradient minimization until convergence was reached, at which time constraints were gradually removed. Molecular dynamics simulations (100 ps) at 300 K and mechanics (2 × 1000 cycles of conjugate-gradient minimization) were performed using DISCOVER. The resulting structure subsequently served as the starting structure for additional energy refinement, docking, molecular dynamics, and complex formation.

A model of the complex of QQ58 with G-quadruplex was built and energy-minimized using a protocol similar to that described for G-quadruplex structures. Low-energy structures were manually docked into the intercalation site, and energies were computed using AFFINITY. To clarify the orientation

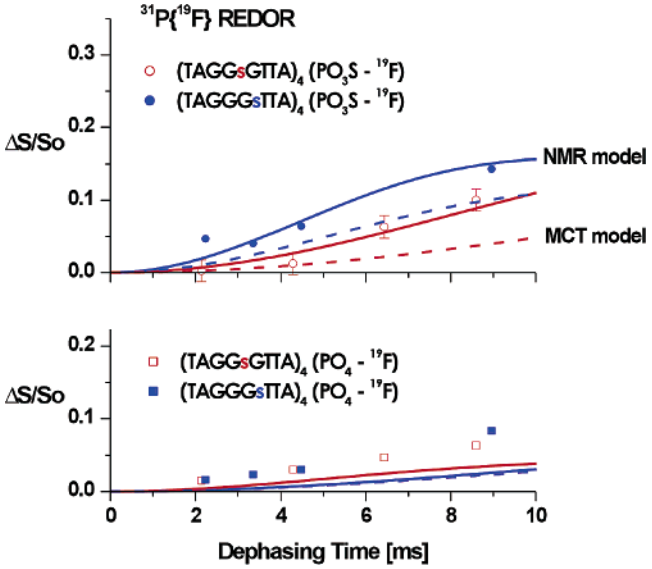

FIGURE 3: $^{31}P\{^{19}F\}$ REDOR dephasing ($\Delta S/S_0$) for two G-quadruplex−drug complexes. Dephasing for the $^{31}PO_3S$ of TAGGGsTTA (top, ●) and TAGGsGTTA (top, ○) is consistent with the predictions (—) of the NMR model shown in Figures 6 and 7 but not those of the MCT model of Duan et al. (2001) (···). Both models predict somewhat less dephasing than is observed for the $^{31}PO_4$ groups (bottom, □ and ■). Predicted dephasing has been scaled by 32% to account for incomplete binding. Error bars are based on signal−noise determinations.

of the ligands in the intercalation site, the electrostatic potentials at the van der Waals surface of the G-quadruplex were determined by solvent-surface calculations. Thus, orientations with low intermolecular potential energy were obtained while moving ligand and ligand-binding G-tetrad residues. The resulting ligand−G-quadruplex complex trajectories were energy-minimized using 1000 cycles of conjugate-gradient minimizer, and the interaction energies were computed. The resulting structure is referred to in the text as the MCT model, identifying the journal in which the model first appeared (*10*).

An NMR model was built starting with the MCT coordinates and performing energy-minimized dynamics simulations as described above but now restrained by the $^{13}CH_3-^{19}F$ and $^{31}PO_3S-^{19}F$ REDOR dephasing. This was an interactive process. The dephasing was calculated (*23*) using the positions of the ^{19}F relative to the 4 $^{31}PO_3S$ groups and 24 $^{31}PO_4$ groups of d(TAGGsGTTA)$_4$. For d(TAGGGsTTA)$_4$, the positions of the 4 $^{13}CH_3$ thymidine labels were included. These positions were altered empirically to improve the match between calculated and observed dephasing, and the resulting structure was allowed to rearrange locally in a molecular dynamics simulation to find a more energy-favorable orientation. Altogether, six iterations were performed to find a reasonable match between the experimental and calculated dephasing.

RESULTS AND DISCUSSION

REDOR Dephasing. The $^{31}P\{^{19}F\}$ REDOR spectra of the QQ58 complex with d(TAGGsGTTA)$_4$ are shown in the top two panels of Figure 2. The $^{31}PO_4$ centerband is at −3 kHz (arbitrary reference); all of the other major peaks in the full-echo spectrum are $^{31}PO_4$ spinning sidebands. The sulfur substitution from phosphorothioation (*24*) results in a 56-

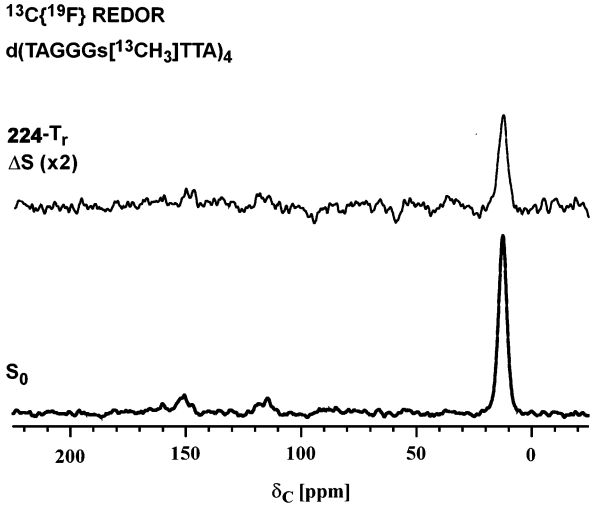

FIGURE 4: $^{13}C\{^{19}F\}$ REDOR NMR spectra (125 MHz) of the complex of QQ58 with a ^{13}C-methyl-labeled T6 quadruplex. The top spectrum is the REDOR difference after 224 rotor cycles of dipolar evolution with magic-angle spinning at 7463 Hz and xy-8 phase cycling for both ^{13}C and ^{19}F pulses. The bottom spectrum is the full echo. For long evolution times, only the methyl-carbon peak at 12 ppm has a long enough T_2 to result in strong signals. Data acquisition required 1 day of spectral accumulation.

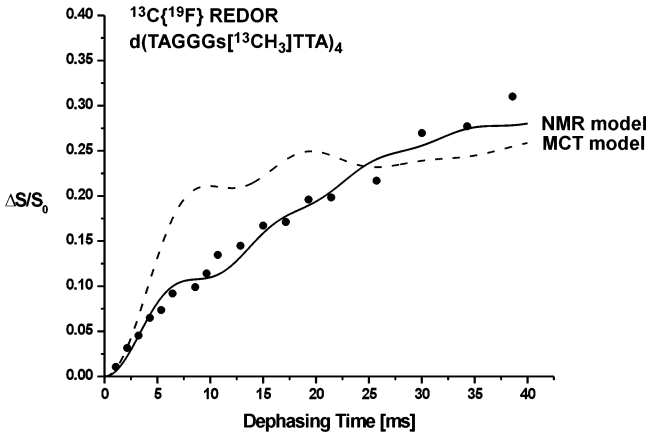

FIGURE 5: $^{13}C\{^{19}F\}$ REDOR dephasing ($\Delta S/S_0$) for the quadruplex complex of Figure 3. The experimental dephasing (●) matches that expected (—) from the NMR model shown in Figures 6 and 7 but not that of the MCT model of Duan et al. (*10*) (···). The calculated dephasing has been scaled by 32% to account for incomplete binding.

ppm downfield shift of the $^{31}PO_3S$ signal (*25*), which is easy to detect despite the reduction in intensity by a factor of 6 relative to the $^{31}PO_4$ signal. The shift puts the $^{31}PO_3S$ centerband at +8 kHz. Because relative REDOR dephasing rates of the sidebands contain information about the orientation of the P−F vector relative to the ^{31}P chemical-shift tensor (*23*), both distance and orientation can in principle be determined in the same experiment, which was our original intention for the $^{31}PO_3S-^{19}F$ dephasing. However, the spectra of Figure 2 were ultimately too noisy to accomplish this. Instead, the center- and sidebands were folded together to improve sensitivity in the determination of total dephasing (bottom two panels of Figure 2). Higher sensitivity for distance determinations could have been achieved by faster spinning; the collapse of sidebands into the centerband by spinning is preferred to the folding of sidebands into the centerband by synchronous sampling. However, care must

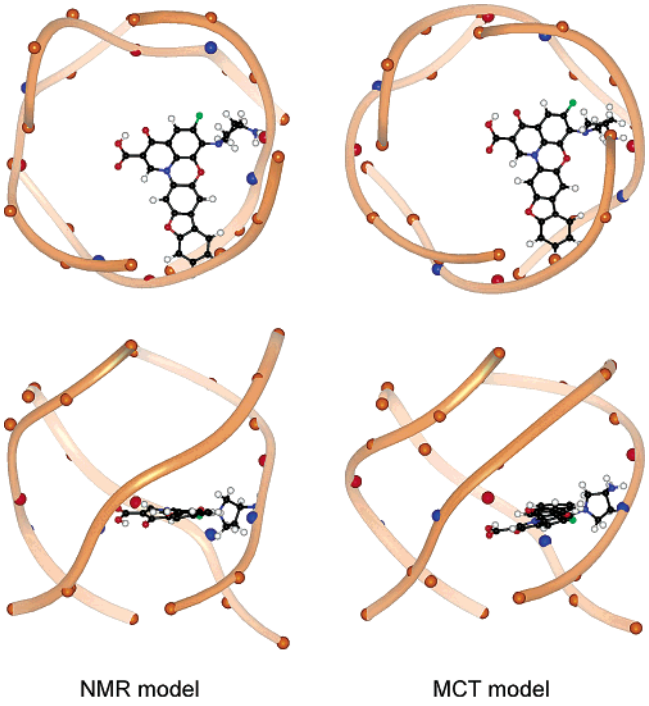

FIGURE 6: Two views (top and side) of the NMR model (left column) and the MCT model (right column) of Duan et al. of the QQ58 quadruplex complex. The tubes represent the DNA backbones and pass through the phosphates, shown as large orange spheres. The PO_3S groups are in blue (TAGGGsTTA) and red (TAGGsGTTA). The fluorine of QQ58 is shown in green, carbons in black, and the oxygens in red (all small spheres).

be taken to avoid a rotational-resonance condition (*26*), resulting from the overlap of the $^{31}PO_4$ spinning sidebands with the $^{31}PO_3S$ centerband. This would have required a spinning speed of 14 kHz, which was not possible with our 5-mm rotors.

The $^{31}P\{^{19}F\}$ REDOR dephasing ($\Delta S/S_0$) for QQ58 complexed to $d(TAGGsGTTA)_4$ and $d(TAGGGsTTA)_4$ as a function of the dipolar evolution time is shown in Figure 3. Binding below the G5-tetrad plane leads to an increased coupling of the ^{19}F with the $^{31}PO_3S$ groups of the $d(TAGGGsTTA)_4$ complex relative to that of the corresponding groups of the $d(TAGGsGTTA)_4$ complex. The $^{31}PO_3S$ dephasing for the $d(TAGGGsTTA)_4$ complex is consistently greater than that for the $d(TAGGsGTTA)_4$ complex. This result proves that binding of the drug is below the G5-tetrad plane. Binding at this site had been surmised by Fedoroff et al. (*9*) based on just chemical shifts and modeling. No corrections were made to the values for the $^{31}P\{^{19}F\}$ dephasing (*20*), even though only a single ^{31}P π pulse was used, because only relative REDOR dephasing rates are important for the modeling described below.

The $^{13}C\{^{19}F\}$ REDOR spectra of the $d(TAGGGsTTA)_4$ complex (with the methyl of T6 ^{13}C labeled) are dominated by the methyl-carbon peak (Figure 4). The total dephasing has a strong dependence on the evolution time for the first 5 ms and then weakens as the dephasing reaches a final value estimated at 32% (Figure 5). We attribute the lack of full dephasing to free QQ58. That is, only 32% of the quadruplex is complexed. This conclusion is consistent with the solution-state ^1H NMR spectra used to monitor the titration of $d(TAGGGsTTA)_4$ with QQ58 (*10*). Both free and bound quadruplex imino protons were observed throughout the titration. At 1:1 molar ratio of quadruplex/QQ58, the bound-version G5 imino proton intensity was less than half that of the starting free G5 intensity (*10*).

Modeling. The structural information provided by the REDOR results of Figures 3 and 5 led to substantive changes in the MCT model. In particular, the two closest $^{31}PO_3S-^{19}F$ distances had to be significantly shorter than had been

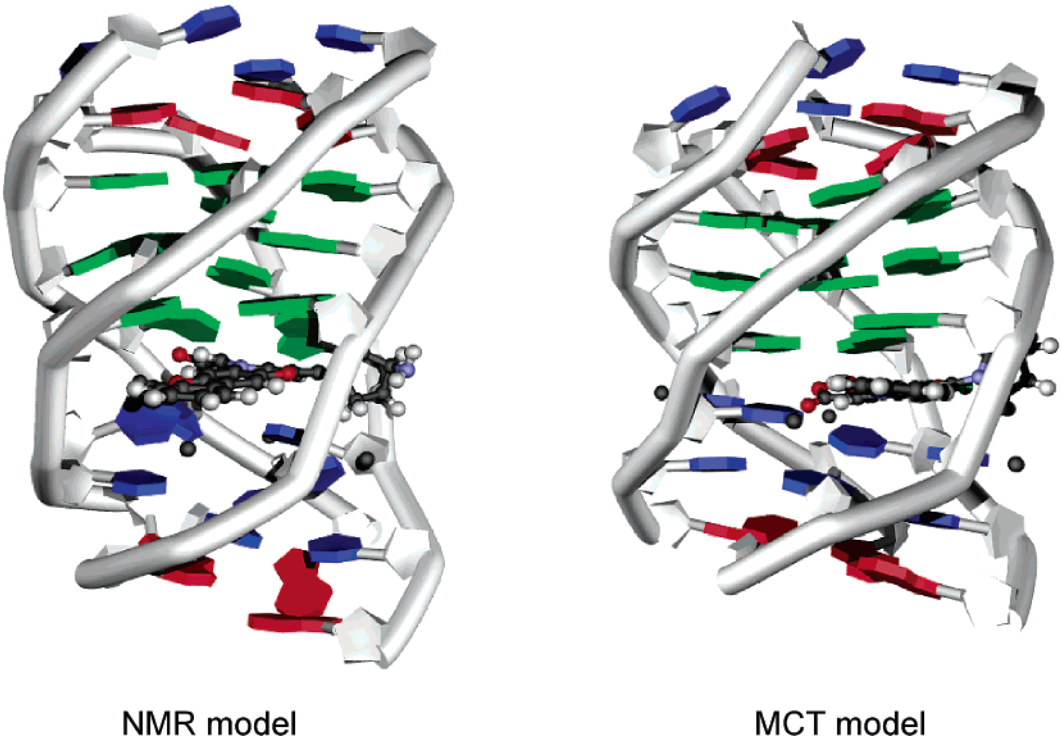

FIGURE 7: Orientations of the bases in the NMR and MCT models of the QQ58 quadruplex complex. G is in green, T in blue, and A in red. The thymidine methyl ^{13}C labels are shown as isolated black spheres next to the thymidine bases. This cartoon of the complex was created in Accelrys DS Viewer Pro.

Table 1: Comparison of NMR and MCT Models of G-Quadruplex Complexes with QQ58

internuclear pair	distance in NMR model (Å)		distance in MCT model (Å)	
	G5[a]	T6[b]	G5[a]	T6[b]
$^{31}PO_3S-^{19}F$	7.6	6.1	8.5	6.5
	7.9	7.1	10.6	9.1
	15.3	15.0	17.3	16.7
	16.0	15.3	19.4	18.4
$^{13}CH_3-^{19}F$		4.8		5.0
		7.8		5.2
		9.0		6.7
		10.7		12.7

[a] d(TAGGsGTTA)$_4$. [b] d(TAGGGsTTA)$_4$.

proposed in the MCT model to match the observed $^{31}P\{^{19}F\}$ dephasing (error bars of Figure 3). The NMR restraints (Table 1) move QQ58 closer to the middle of the quadruplex (Figure 6) and alter the orientation of the rings of the bases forming the G5 tetrad and, to a lesser extent, the G4 tetrad (Figure 7). Even though the *absolute* total dephasing is small, the *relative* difference in dephasing between the two models is typically 50%. The $^{31}PO_4$-^{19}F REDOR results were not helpful in refining the NMR model.

After 7 ms of dipolar evolution, the $^{13}C\{^{19}F\}$ dephasing ($\Delta S/S_0$), has an apparent initial plateau of 0.09 (Figure 5). This indicates that one of the four $^{13}CH_3-^{19}F$ distances is short, while the other three are much longer. This result is inconsistent with the distances in the MCT model (Table 1). The MCT model has the QQ58 ^{19}F equally close to two $^{13}CH_3$ groups; hence, the predicted dephasing reaches an initial plateau twice that of the experimentally observed value (Figure 5). To match the $^{13}C\{^{19}F\}$ dephasing at long evolution times, the longest $^{13}C-^{19}F$ distances had to be reduced. As a result, the thymidine bases farthest from the ^{19}F undergo a significant roll and twist (Figure 8), and all of the thymidines move closer to the center of the quadruplex. The twist may be responsible for the altered packing of the G4 and G5 bases.

These results are consistent with the ^1H solution-state NMR of the guanine imino protons (*10*). Intramolecular hydrogen bonding involving the imino protons of the G tetrads results in slow exchange with the water protons (*27*). The disappearance of the unbound G5 imino proton resonance in the QQ58−DNA complex (*10*) could then be due to the disruption of the G5 tetrad hydrogen-bonding network, allowing for facile exchange with solvent water.

The overall length of the quadruplex is increased although not its width, even though, at several places, the sugar−phosphate backbone is noticeably bulged (top left of Figure 6). This change in shape is unlikely to be due to the phosphorothioate substitution because a sulfur is about the same size as an oxygen (the van der Waals radius of the sulfur is about 0.4 Å larger) and does not change the charge of the phosphate group (*28*).

The shape of the drug−DNA complex shown in Figures 6 and 7 was determined using REDOR resulting from the direct measurement of distances from DNA to the drug. In related work, Olsen et al. (*29*) have examined distamycin−DNA binding indirectly by using $^{31}P\{^{19}F\}$ REDOR to monitor the DNA minor grove as a function of the drug−DNA stoichiometry.

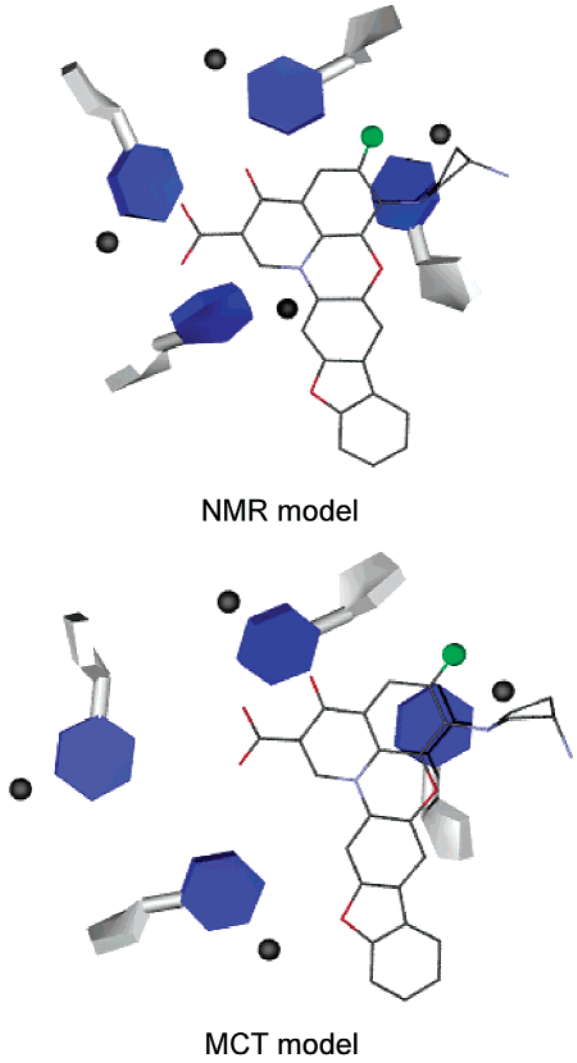

FIGURE 8: Top view of the T6 bases in the NMR and MCT models. The thymidine bases are in blue, and QQ58 is drawn with lines. The thymidine methyl ^{13}Cs are shown as black spheres, and the ^{19}Fs are shown as green spheres.

Water. The NMR sample was kept free from adventitious water by means of molecular-sieve end caps. When this was not done, the sample slowly hydrated. The net result was large-amplitude molecular motion that shrunk the ^{31}P chemical-shift tensors and partially averaged the weak $^{31}P-^{19}F$ and $^{13}C-^{19}F$ dipolar couplings essential to REDOR analysis. The lyophilized samples of Figures 2 and 4 were not dehydrated; structural water accounted for some 10% of the total sample weight. Nevertheless, the structure determined by REDOR was of a static complex, which represents perhaps the most tightly bound form of QQ58. We have no way of knowing how this static structure relates to the time average of the dynamic structure in solution. This is a familiar problem in solid-state characterization that is faced by crystallographers all of the time.

ACKNOWLEDGMENT

This work was supported by NIH Grants CA49751 (to L.H.H.) and EB01964 (to J.S.).

REFERENCES

1. Gellert, M., Lipsett, M. N., and Davies, D. R. (1962) Helix Formation by Guanylic Acid, *Proc. Natl. Acad. Sci. U.S.A.*, 48, 2013−2018.

2. Hurley, L. H. (1989) DNA and Associated Targets for Drug Design, *J. Med. Chem. 32*, 2027−2033.
3. Sun, D., Thompson, B., Cathers, B. E., Salazar, M., Kerwin, S. M., Trent, J. O., Jenkins, T. C., Neidle, S., and Hurley, L. H. (1997) Inhibition of Human Telomerase by a G-Quadruplex-Interactive Compound, *J. Med. Chem. 40*, 2113−2116.
4. Read, M. A., Wood, A. A., Harrison, R. J., Gowan, S. M., Kelland, L. R., Dosanjh, H. S., and Neidle, S. (1999) Molecular Modeling Studies on G-Quadruplex Complexes of Telomerase Inhibitors: Structure−Activity Relationships, *J. Med. Chem. 42*, 4538−4546.
5. Izbicka, E., Wheelhouse, R. T., Raymond, E., Davidson, K. K., Lawrence, R. A., Sun, D., Windle, B. E., Hurley, L. H., and Von Hoff, D. D. (1999) Effects of Cationic Porphyrins as G-Quadruplex-Interactive Agents in Human Tumor Cells, *Cancer Res. 59*, 639−644.
6. Riou, J.-F., Mailliet, P., Laoui, A., Renou, E., Petigenet, O., Guittat, L., and Mergny, J.-L. (2001) Apoptosis, Cell Senescence, and Telomere Shortening Induced by a New Series of Specific G-Quadruplex DNA Ligands, *Proc. Am. Assoc. Cancer Res. 42*, 837.
7. Siddiqui-Jain, A., Grand, C. L., Bearss, D. J., and Hurley, L. H. (2002) Direct Evidence for a G-Quadruplex in a Promoter Region and Its Targeting with a Small Molecule To Repress c-*MYC* Transcription, *Proc. Natl. Acad. Sci. U.S.A. 99*, 11593−11598.
8. Smith, F. W., and Feigon, J. (1993) Strand Orientation in the DNA Quadruplex Formed from the Oxytricha Telomere Repeat Oligonucleotide d($G_4T_4G_4$) in Solution, *Biochemistry 32*, 8682−8692.
9. Fedoroff, O. Yu., Salazar, M., Han, H., Chemeris, V. V., Kerwin, S. M., and Hurley, L. H. (1998) NMR-Based Model of a Telomerase-Inhibiting Compound Bound to G-Quadruplex DNA, *Biochemistry*, *37*, 12367−12374.
10. Duan, W., Rangan, A., Vankayalapati, H., Kim, M.-Y., Zeng, Q., Sun, D., Han, H., Fedoroff, O. Yu., Nishioka, D., Sun, Y. R., Izbicka, E., Von Hoff, D. D., and Hurley, L. H. (2001) Design and Synthesis of Fluoroquinophenoxazines that Interact with Human Telomeric G-Quadruplexes and Their Biological Effects, *Mol. Cancer Ther. 1*, 103−120.
11. Gullion, T., and Schaefer, J. (1989) Detection of Weak Heteronuclear Dipolar Coupling by Rotational-Echo Double-Resonance NMR, *Adv. Magn. Reson. 13*, 58−83.
12. McDowell, L. M., and Schaefer, J. (1996) High-Resolution NMR of Biological Solids, *Curr. Opin. Struct. Biol. 6*, 624−629.
13. McDowell, L. M., McCarrick, M. A., Studelska, D. R., O'Connor, R. D., Light, D. R., Guilford, W. J., Arnaiz, D., Dallas, J. L., Poliks, B., and Schaefer, J. (2003a) Human Factor Xa Bound Amidine Inhibitor Conformation by Double Rotational-Echo Double-Resonance Nuclear Magnetic Resonance and Molecular Dynamics Simulations, *J. Med. Chem. 46*, 359−363.
14. McDowell, L. M., Poliks, B., Studelska, D. R., O'Connor, R. D., Beusen, D. D., and Schaefer, J. (2004) Rotational-Echo Double-Resonance NMR-Restrained Model of the Ternary Complex of 5-Enolpyruvylshikimate-3-phosphate Synthase, *J. Biomol. NMR 28*, 11−29.
15. Balbach, J. J., Ishii, Y., Antzutkin, O. N., Leapman, R. D., Rizzo, N. W., Dyda, F., Reed, J., and Tycko, R. (2000) Amyloid Fibril Formation by Aβ16−22, a Seven-Residue Fragment of the Alzheimer's β-Amyloid Peptide, and Structural Characterization by Solid State NMR, *Biochemistry 39*, 13748−13759.
16. Smith, S. O., Kawakami, T., Liu, W., Ziliox, M., and Aimoto, S. (2001) Helical Structure of Phospholamban in Membrane Bilayers, *J. Mol. Biol. 313*, 139−1148.
17. Kim, S. J., Cegelski, L., Studelska, D. R., O'Connor, R. D., Mehta, A. K., and Schaefer J. (2002) Rotational-Echo Double Resonance Characterization of the Effects of Vancomycin on Cell Wall Synthesis in *Staphylococcus aureus*, *Biochemistry 41*, 6967−6977.
18. Schaefer, J., and McKay, R. A. (1999) Multi-tuned Single Coil Transmission Line Probe for Nuclear Magnetic Resonance Spectrometer, U.S. Patent 5,861,748.
19. Gullion, T., Baker, D. B., and Conradi, M. S. (1990) New, Compensated Carr−Purcell Sequences, *J. Magn. Reson. 89*, 479−484.
20. Weldeghiorghis, T. K., and Schaefer, J. (2003) Compensating for Pulse Imperfections in REDOR, *J. Magn. Reson. 165*, 230−236.
21. Bennett, A. E., Rienstra, C. M., Auger, M., Lakshmi, K. V., and Griffin, R. G. (1995) Heteronuclear Decoupling in Rotating Solids, *J. Chem. Phys. 103*, 6951−6958.
22. Wang, Y., and Patel, D. J. (1993) Solution Structure of the Human Telomeric Repeat d[$AG_3(T_2AG_3)_3$]G-tetraplex, *Structure 1*, 263−282.
23. O'Connor, R. D., and Schaefer, J. (2002) Relative CSA-Dipolar Orientation from REDOR Sidebands, *J. Magn. Reson. 154*, 46−52.
24. Eckstein, F., and Jovin, T. M. (1983) Assignment of Resonances in the Phosphorus-31 Nuclear Magnetic Resonance Spectrum of poly[d(A−T)] from Phosphorothioate Substitution, *Biochemistry 22*, 4546−4550.
25. Merritt, M. E., Sigurdsson, S. T., and Drobny, G. P. (1999) Long-Range Distance Measurements to the Phosphodiester Backbone of Solid Nucleic Acids Using ^{31}P-^{19}F REDOR NMR, *J. Am. Chem. Soc. 121*, 6070−6071.
26. Raleigh, D. P., Levitt, M. H., and Griffin R. G. (1988) Rotational Resonance in Solid-State NMR, *Chem. Phys. Lett. 146*, 71−76.
27. Wang, Y., and Patel, D. J. (1992) Guanine Residues in d(T_2AG_3) and d(T_2G_4) From Parallel-Stranded Potassium Cation Stabilized G-Quadruplexes with Anti-Glycosidic Torsion Angles in Solution, *Biochemistry 31*, 263−282.
28. Stivers, J. T., Nawrot, B., Stec, W. J., Jagadeesch, G. J., and Shuman, S. (2000) Stereochemical Outcome and Kinetic Effects of *R*p- and *S*p-Phosphorothioate Substitutions at the Cleavage Site of Vaccinia Type I DNA Topoisomerase, *Biochemistry 39*, 5561−5572.
29. Olsen, G. L., Louie, E. A., Drobny, G. P., and Sigurdsson, S. Th. (2003) Determination of DNA Minor Goove Width in Distamycin−DNA Complexes by Solid-State NMR, *Nucleic Acid Res. 31*, 5084−5089.

BI049697H